

# SCALING LAWS FOR DIFFUSION TRANSFORMERS

**Anonymous authors**

Paper under double-blind review

## ABSTRACT

Diffusion transformers (DiT) have already achieved appealing synthesis and scaling properties in content recreation, *e.g.*, image and video generation. However, scaling laws of DiT are less explored, which usually offer precise predictions regarding optimal model size and data requirements given a specific compute budget. Therefore, experiments across a broad range of compute budgets, from  $1e17$  to  $6e18$  FLOPs are conducted to confirm the existence of scaling laws in DiT *for the first time*. Concretely, the loss of pretraining DiT also follows a power-law relationship with the involved compute. Based on the scaling law, we can not only determine the optimal model size and required data but also accurately predict the text-to-image generation loss given a model with 1B parameters and a compute budget of  $1e21$  FLOPs. Additionally, we also demonstrate that the trend of pre-training loss matches the generation performances (*e.g.*, FID), even across various datasets, which complements the mapping from compute to synthesis quality and thus provides a predictable benchmark that assesses model performance and data quality at a reduced cost.

## 1 INTRODUCTION

Scaling laws in large language models (LLMs) (Kaplan et al., 2020; Hestness et al., 2017; Henighan et al., 2020; Hoffmann et al., 2022) have been widely observed and validated, suggesting that pre-training performance follows a power-law relationship with the compute  $C$ . The actual compute could be roughly calculated as  $C = 6ND$ , where  $N$  is the model size and  $D$  is the data quantity. Therefore, determining the scaling law helps us make informed decisions about resource allocation to maximize computational efficiency, namely, figure out the optimal balance between model size and training data (*i.e.*, the optimal model and data scale) given a fixed compute budget. However, scaling laws in diffusion models remain less explored.

The scalability has already been demonstrated in diffusion models, especially for diffusion transformers (DiT). Specifically, several prior works (Mei et al., 2024; Li et al., 2024) reveal that larger models always result in better visual quality and improved text-image alignment. However, the scaling property of diffusion transformers is *clearly observed but not accurately predicted*. Besides, the absence of explicit scaling laws also hinders a comprehensive understanding of how training budget relate to model size, data quantity, and loss. As a result, we cannot determine accordingly the optimal model and data sizes for a given compute budget and accurately predict training loss. Instead, heuristic configuration searches of models and data are required, which are costly and challenging to ensure optimal balance.

In this work, we characterize the scaling behavior of diffusion models for text-to-image synthesis, resulting in the explicit scaling laws of DiT *for the first time*. To investigate the explicit relationship between pretraining loss and compute, a wide range of compute budgets from  $1e17$  to  $6e18$  FLOPs are used. Models ranging from 1M to 1B are pretrained under given compute budgets. As shown in Fig. 1, for each compute budget, we can fit a parabola and extract an optimal point that corresponds to the optimal model size and consumed data under that specific compute constraint. Using these optimal configurations, we derive scaling laws by fitting a power-law relationship between compute budgets, model size, and training loss. To evaluate the derived scaling laws, we extrapolate the compute budget to  $1.5e21$  FLOPs that results in the compute-optimal model size (approximately 1B parameters) and the corresponding data size. Therefore, a 1B-parameter model is trained under this budget and the final loss matches our prediction, demonstrating the effectiveness and accuracy of our scaling laws.

054  
055  
056  
057  
058  
059  
060  
061  
062  
063  
064  
065  
066  
067  
068  
069  
070  
071  
072  
073  
074  
075  
076  
077  
078  
079  
080  
081  
082  
083  
084  
085  
086  
087  
088  
089  
090  
091  
092  
093  
094  
095  
096  
097  
098  
099  
100  
101  
102  
103  
104  
105  
106  
107

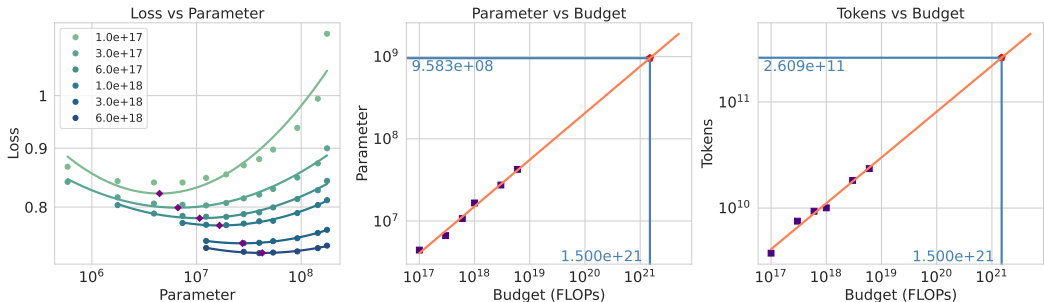


Figure 1: **IsoFLOP and Model/Data Scaling Curves.** For each training budget, we train multiple models of varying sizes. A parabola is fitted to the loss for each training budget, and the minimum point on each parabola (represented by the purple dots) corresponds to the optimal allocation of model size and data for that specific budget. By identifying the model and data sizes at these optimal points, we can plot the scaling trends of model parameters, tokens, and training budgets. The power-law curves shown allow us to predict the optimal configurations for larger compute budgets, such as  $1.5e21$  FLOPs.

To make the best use of the scaling laws, we demonstrate that the generation performances (*e.g.*, FID (Fréchet Inception Distance)) also match the trend of pretraining loss. Namely, the synthesis quality also follows the power-law relationship with the compute budget, making it predictable. More importantly, this observation is transferable across various datasets. We conduct additional experiments on the COCO validation set (Lin et al., 2015), and the same scaling patterns hold, even when tested on out-of-domain data. Accordingly, scaling laws could serve as a predictable benchmark where we can assess the quality of both models and datasets at a significantly reduced computational cost, enabling efficient evaluation and optimization of the model training process.

To summarize, we at first confirm the presence of scaling laws in diffusion transformers during training, revealing a clear power-law relationship between compute budget and training losses. Next, we establish a connection between pretraining loss and synthesis evaluation metrics. Finally, we conducted preliminary experiments that demonstrate the potential of using scaling laws to evaluate both data and model performance. By conducting scaling experiments at a relatively low cost, we can assess and validate the effectiveness of different configurations based on the fitted power-law coefficients.

## 2 RELATED WORK

**Diffusion Transformers** Transformers have become the de facto model architecture in language modeling (Radford, 2018; Radford et al., 2019; Devlin et al., 2019), and they have also achieved significant success in computer vision tasks (Dosovitskiy et al., 2021; He et al., 2021). Recently, Transformers have been introduced into diffusion models (Peebles & Xie, 2023), where images are divided into patches (tokens), and the diffusion process is learned on these tokens. Additional conditions, such as timestep and text, are incorporated into the network via cross-attention (Chen et al., 2023), Adaptive Normalization (Perez et al., 2017), or by concatenating them with image tokens (Bao et al., 2023). Zheng et al. (2023) proposed masked transformers to reduce training costs, while Lu et al. (2024) introduced techniques for unrestricted resolution generation. Diffusion Transformers (DiTs) inherit the scalability, efficiency, and high capacity of Transformer architectures, positioning them as a promising backbone for diffusion models. Motivated by this scalability, we investigate the scaling laws governing these models in this work. To ensure robust and clear conclusions, we adopt a vanilla Transformer design (Vaswani et al., 2023), using a concatenation of image, text, and time tokens as input to the models.

**Scaling Laws** Scaling laws (Hestness et al., 2017) have been fundamental in understanding the performance of neural networks as they scale in size and data. This concept has been validated across several large pretraining models (Dubey et al., 2024; Bi et al., 2024; Achiam et al., 2023). Kaplan et al. (2020); Henighan et al. (2020) were the first to formalize scaling laws in language

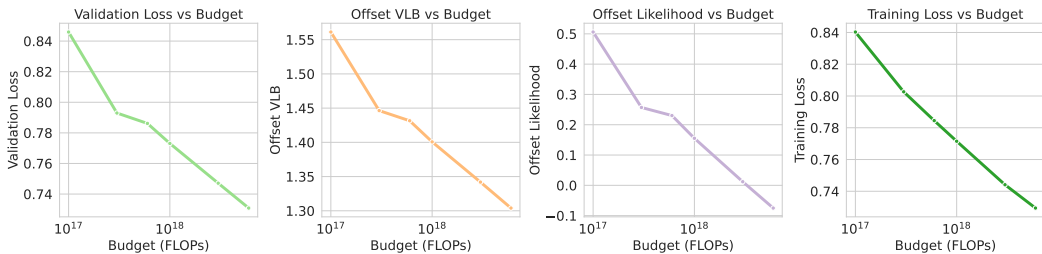


**Figure 2: Scaling Curves for Different Metrics.** We present the scaling curves for training and validation loss, offset VLB, and offset likelihood. Validation metrics are evaluated on the COCO 2014 validation set. The metrics display consistent trends and similar shapes, all adhering to a power-law relationship. This demonstrates that each of these metrics can be used to observe scaling laws effectively. For simplicity, we primarily focus on training loss in subsequent analyses.

models and extend them to autoregressive generative models, demonstrating that model performance scales predictably with increases in model size and dataset quantity. Hoffmann et al. (2022) further highlighted the importance of balancing model size and dataset size to achieve optimal performance. In the context of diffusion models, prior works (Mei et al., 2024; Li et al., 2024) have empirically demonstrated their scaling properties, showing that larger compute budgets generally result in better models. These studies also compared the scaling behavior of various model architectures and explored sampling efficiency. However, no previous works provide an explicit formulation of scaling laws for diffusion transformers to capture the relationship between compute budget, model size, data, and loss. In this paper, we aim to address this gap by systematically investigating the scaling behavior of diffusion transformers (DiTs), offering a more comprehensive understanding of their scaling properties.

### 3 METHOD

#### 3.1 BASIC SETTINGS

Unless otherwise stated, all experiments in this paper adhere to the same basic settings. While the training techniques and strategies employed may not be optimal, they primarily affect the scaling coefficients rather than the scaling trends. In this section, we outline the critical settings used in our experiments. Additional details are provided in Appendix C.

**Diffusion Formulation** All experiments are conducted using the Rectified Flow (RF) formulation (Liu et al., 2022; Lipman et al., 2022; Albergo et al., 2023) with v-prediction. For timestep sampling, we adopt the Logit-Normal (LN) Sampling scheduler  $\pi_{ln}(t; m, s)$ , as proposed in Esser et al. (2024). A detailed ablation study of this choice can be found in Appendix F.1.

**Models & Dataset** As noted in Kaplan et al. (2020), the model design does not significantly impact scaling trends unless the architecture is extremely shallow or slim. We employ a vanilla transformer architecture (Vaswani et al., 2023) with minimal modifications. The text, image, and timestep tokens are concatenated as input (in-context conditioning (Peebles & Xie, 2023)). A dataset of 108 million image-text pairs is randomly sampled from Laion-Aesthetic (Schuhmann et al., 2022). This subset is then re-captioned using LLAVA 1.5 (Liu et al., 2024). A validation set consisting of 1 million pairs is created from this subset. Further details can be found in Appendix C.1 and C.2.

**Scaling Metrics** A natural question arises when investigating scaling laws during training: *What metrics should be selected to observe scaling behavior?* In the context of Large Language Models (LLMs), the standard approach is autoregressive training (Radford, 2018; Radford et al., 2019), where the model is trained to predict the next token in a sequence, directly optimizing the likelihood of the training data. This has proven to be a reliable method for measuring model performance as the compute budget scales up. Inspired by this approach, we extend the concept of scaling laws to diffusion models, using **loss** and **likelihood** as our key metrics.

**Loss** is the primary metric chosen to observe scaling behavior during training. Unlike autoregressive models, diffusion models do not directly optimize likelihood. Instead, the objective is to match a time-conditioned velocity field (Ma et al., 2024; Liu et al., 2022; Lipman et al., 2022; Albergo et al., 2023). Specifically, the velocity  $\mathbf{v}(x_t, t)$  at timestep  $t$  is defined as:

$$\mathbf{v}(x_t, t) = x'_t = \alpha'_t x_0 + \beta'_t \epsilon, \quad (1)$$

where  $x_0$  represents the original data and  $\epsilon$  denotes the noise. Here, the prime symbol  $'$  indicates the derivative with respect to time  $t$ . In the rectified flow framework, the coefficients  $\alpha_t$  and  $\beta_t$  are defined as  $\alpha_t = 1 - t, \beta_t = t$ . Thus, the velocity  $\mathbf{v}$  can be further simplified as:

$$\mathbf{v}(x_t, t) = -x_0 + \epsilon. \quad (2)$$

The corresponding loss function is expressed in terms of the expected value:

$$\mathcal{L}(\theta, \mathbf{x}, t) = \mathbb{E}_{t \sim [1, T], \epsilon \sim \mathcal{N}(0, I)} \left[ \|\mathbf{v}_\theta(x_t, t) + x_0 - \epsilon\|^2 \right] \approx \frac{1}{N} \sum_{i=1}^N \left[ \|\mathbf{v}_\theta(x_t, t) + x_0 - \epsilon\|^2 \right]. \quad (3)$$

The **training loss** is estimated using a Monte Carlo method, which involves timesteps and noise sampling. The stochasticity inherent in this process can cause significant fluctuations, which are mitigated by employing a larger batch size of 1024 and applying Exponential Moving Average (EMA) smoothing. In our experiments, we set  $\alpha_{\text{EMA}} = 0.9$ , which is found to produce stable results. A detailed ablation study on the choice of EMA coefficients is provided in Appendix F.2. This smoothing procedure helps reduce variance and provides clearer insights into training dynamics.

In addition to the training loss, **validation loss** is also computed on the COCO 2014 dataset (Lin et al., 2015). To ensure consistency with the training loss, timesteps are sampled using the LN timestep sampler  $\pi_{ln}(t; m, s)$ , and evaluation is performed on 10,000 data points, with 1,000 timesteps sampled per point.

**Likelihood** is our secondary metric. The likelihood over the dataset distribution  $P_{\mathcal{D}}$  given model parameters  $\theta$  is represented as  $\mathbb{E}_{x \sim P_{\mathcal{D}}} [p_\theta(x)]$ , which can be challenging to compute directly. In this paper, we measure likelihood using two different methods. The first method is based on the Variational Autoencoder (VAE) framework (Kingma et al., 2021; Song et al., 2021a; Vahdat et al., 2021), which approximates the lower bound of log-likelihood using the Variational Lower Bound (VLB). Since the VAE component in our experiments is fixed to Stable Diffusion 1.5, terms related to the VAE remain constant and are ignored in our computation, as they do not affect the scaling behavior. The second method uses Neural Ordinary Differential Equations (ODEs) (Chen et al., 2019; Grathwohl et al., 2018), enabling the computation of exact likelihood through reverse-time sampling.

**Variational Lower Bound (VLB)** We estimate the VLB following the approach in Kingma et al. (2021), where it is treated as a reweighted version of the validation loss. The process starts by converting the estimated velocity into a corresponding estimate of  $x_0$ , after which the loss is computed based on the difference between the estimated  $x_0$  and the original sample. To obtain the VLB, this loss is further reweighted with the weighting coefficient being the derivative of signal-to-noise ratio of noisy samples with respect to time  $t$ , *i.e.*,  $\text{SNR}'(t)$ . More details can be found in Appendix D. All models are evaluated on the COCO 2014 validation set using 10,000 data pairs. For each data point, 1,000 timesteps are sampled to ensure accurate estimations of the VLB.

**Exact Likelihood** The exact likelihood is computed using reverse-time sampling, where a clean sample is transformed into Gaussian noise. The accumulated likelihood transition is calculated using the instantaneous change of variables theorem (Chen et al., 2019):

$$\log p_\theta(x) = \log p_\theta(x_T) - \int_0^T \nabla \cdot f_\theta(x_t, t) dt,$$

where  $f_\theta(x_t, t)$  represents the model’s output, and  $\log p_\theta(x_T)$  is the log density of the final Gaussian noise. The reverse process evolves  $t$  from 0 (data points) to  $T$  (noise). The reverse sampling is performed over 500 steps using the Euler method.

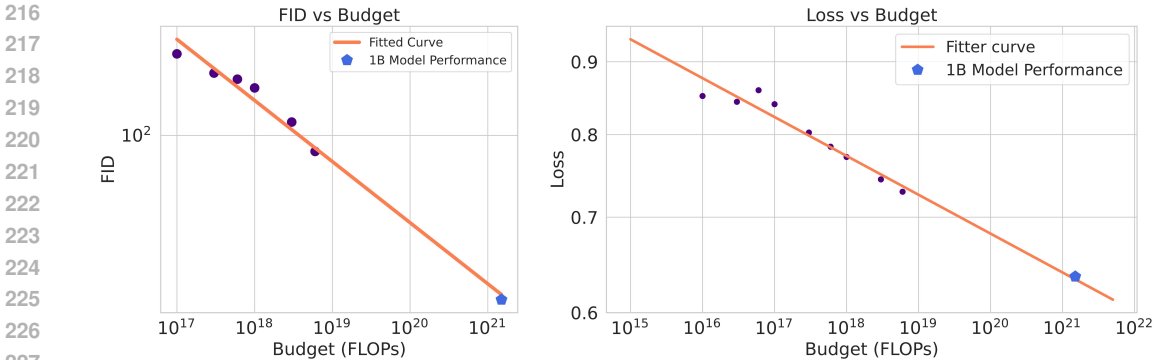


Figure 3: **Performance Scaling Curves.** The plot shows the relationship between training loss, FID, and compute budget, with both axes displayed on a logarithmic scale. The orange lines represent the fitted power-law curves for both metrics across various budgets, while the purple dots mark the performance of compute-optimal models at smaller budgets. In both cases, the blue pentagons indicate the predicted performance at a budget of  $1.5e21$  FLOPs, demonstrating highly accurate predictions for large-scale models.

Following model training, we evaluate models on the validation set to assess their compute-optimal performance. As illustrated in Fig. 2, all four metrics (training loss, validation loss, offset VLB, and offset exact likelihood) exhibit similar trends and shapes as the training budget increases, showing their utility in observing scaling laws. These consistent patterns suggest that any of these metrics can be effectively used to monitor scaling behavior. However, to simplify our experimental workflow, we prioritize **training loss** as the primary metric. Training loss can be observed directly during the training process, without the need for additional evaluation steps, making it a more practical choice for tracking scaling laws in real-time.

### 3.2 SCALING LAWS IN TRAINING DIFFUSION TRANSFORMERS

**Scaling Laws** In this section, we investigate the scaling laws governing diffusion transformers, which describe the relationships between several key quantities: the objective function, model parameters, tokens, and compute. The objective measures discrepancy between the data and model’s predictions. The number of parameters  $N$  reflects model’s capacity, while tokens  $D$  denote the total amount of data (in tokens) processed during training. Compute  $C$ , typically measured in Floating Point Operations (FLOPs), quantifies the total computational resources consumed. In our experiments, the relationship between compute, tokens, and model size is formalized as  $C = 6ND$ , directly linking the number of parameters and tokens to the overall compute budget.

Building on this, we hypothesize that power law equations can effectively capture the scaling relationships between these quantities. Specifically, we represent the optimal model size and token count as functions of the compute budget as follows:

$$N_{\text{opt}} \propto C^a \quad \text{and} \quad D_{\text{opt}} \propto C^b, \tag{4}$$

where  $N_{\text{opt}}$  and  $D_{\text{opt}}$  denote the optimal number of parameters and tokens for a given compute budget  $C$ , with  $a$  and  $b$  as scaling exponents that describe how these quantities grow with compute.

To empirically verify these scaling relationships, following Approach 2 in Hoffmann et al. (2022), we plot the isoFLOP figure to explore scaling laws. We select compute budgets [1e17, 3e17, 6e17, 1e18, 3e18, 6e18]. We change the In-context Transformers from 2 layers to 15 layers. For all experiments, we use AdamW (Kingma & Ba, 2017; Loshchilov & Hutter, 2019) as the default optimizer. Except for the 1B parameter prediction experiments, we apply a constant learning rate of 1e-4. In the 1B parameter experiments, we train the model with a learning rate of 1e-4 for 80% of the total iterations, then decay it to 3.16e-5 for the next 10%, and finally to 1e-5 for the last 10%. This learning rate decay is crucial for larger models, leading to more accurate predictions. Following Wortsman et al. (2023); Team (2024); Molybog et al. (2023), we use a weight decay of 0.01, an epsilon value of 1e-15, and betas [0.9, 0.95]. For all experiments, we employ a batch size

of 1024 and apply gradient clipping with a threshold of 1.0. To enable classifier-free guidance (Ho & Salimans, 2022), we randomly drop the label with a probability of 0.1. During training, we use mixed precision with the BF16 data format.

For each budget, we fit a parabola to the resulting performance curve, as illustrated in Fig. 1, to identify the optimal loss, model size, and data allocation (highlighted by the purple dots). By collecting the optimal values from different budgets and fitting them to a power law, we establish relationships between the optimal loss, model size, data, and compute budgets.

As shown in Fig. 1, except for the  $1e17$  budget, the parabolic fits align closely with the empirical results. This analysis confirms that the optimal number of parameters and tokens scale with the compute budget according to the following expressions:

$$N_{\text{opt}} = 0.0009 \cdot C^{0.5681}, \quad (5)$$

$$D_{\text{opt}} = 186.8535 \cdot C^{0.4319}. \quad (6)$$

In this way, we establish the relationship between compute budget and model/data size. And from the fitted scaling curves, we observe that the ratio between the scaling exponent for data and the scaling exponent for model size is  $0.4319/0.5681$ . This indicates that, under our specific settings, both the model and data sizes need to increase in tandem as the training budget increases. However, the model size grows at a slightly faster rate compared to the data size, as reflected by the proportional relationship between the two exponents.

Additionally, in Fig. 3, we fit the relationship between the compute budget and loss, which follows the equation:

$$L = 2.3943 \cdot C^{-0.0273}. \quad (7)$$

To validate the accuracy of these fitted curves, we calculate the optimal model size (958.3M parameters) and token count for a compute budget of  $1.5e21$ . A model is then trained with these specifications to compare its training loss with the predicted value. As demonstrated in Fig. 3, this model’s training loss closely matches the predicted loss, further confirming the validity of our scaling laws.

### 3.3 PREDICTING GENERATION PERFORMANCE

In generative tasks, relying solely on training loss to evaluate performance often falls short of capturing the perceptual quality of generated images. Training loss does not fully reflect how closely the generated images resemble real ones or how well they align with textual prompts in terms of content and style. To address this limitation, the Fréchet Inception Distance (FID) is commonly used to evaluate image quality.

**Fréchet Inception Distance (FID)** FID measures the distance between the distributions of generated and real images in a feature space, with lower FID values indicating higher image quality. For our experiments, we utilize compute-optimal models at each training budget, generating samples using the Euler discretization method with 25 steps and a classifier-free guidance (CFG) scale of 10.0. Details on the impact of steps and CFG scale are provided in Appendix F.3. To compute FID, we follow the approach of Sauer et al. (2021), using CLIP features instead of traditional Inception features. Specifically, we employ ViT-L/14 Dosovitskiy et al. (2021) as the vision encoder to extract features from both generated and dataset images and compare their statistics.

**Scaling laws for Performance Predictions** Our analysis reveals that the relationship between FID and the training budget follows a clear power-law trend, as shown in Fig. 3 (left). The relationship is captured by the following equation:

$$\text{FID} = 2.2566 \times 10^6 \cdot C^{-0.234}, \quad (8)$$

where  $C$  is the training budget. The purple dots in the figure represent the FID scores of compute-optimal models at various budgets, and the orange line represents the fitted power-law curve. Notably, the prediction for FID at a large budget of  $1.5e21$  FLOPs (blue pentagon) is highly accurate, confirming the reliability of scaling laws in forecasting model performance even at larger scales. As the compute budget increases, FID values decrease consistently, demonstrating that scaling laws can effectively model and predict the quality of generated images as resources grow.



Figure 4: **Scaling laws for OOD data.** The evaluation of loss, VLB, and NLL are conducted on an out-of-domain dataset COCO 2014 validation set. All metrics decrease monotonically as the budget increases and they share a similar shape. However, a notable shift can be observed. Models have worse performance on the COCO validation set since they are trained on a different data distribution. The shift reflects the differences between datasets.

### 3.4 SCALING LAWS FOR OUT-OF-DOMAIN DATA

Scaling laws remain valid even when models are tested on out-of-domain datasets. To demonstrate this, we conduct validation experiments on the COCO 2014 validation set (Lin et al., 2015), using models that were trained on the Laion5B subset. In these experiments, we evaluate four key metrics: validation loss, Variational Lower Bound (VLB), exact likelihood, and Fréchet Inception Distance (FID). Each metric is tested on 10,000 data points to examine the transferability of the scaling laws across datasets.

The results, as shown in Fig. 4, reveal two key observations:

- Consistent Trends:** Across all four metrics (validation loss, VLB, exact likelihood, and FID), the trends are consistent between the Laion5B subset and the COCO validation dataset. As the training budget increases, model performance improves in both cases, indicating that scaling laws generalize effectively across datasets, regardless of domain differences.
- Vertical Offset:** There is a clear vertical offset between the metrics for the Laion5B subset and the COCO validation dataset, with consistently higher metric values observed on the COCO dataset. This suggests that while scaling laws hold, the absolute performance is influenced by dataset-specific characteristics, such as complexity or distribution. For metrics like validation loss, VLB, and exact likelihood, this offset remains relatively constant across different training budgets. The gap between the FID values for the Laion5B subset and the COCO validation set widens as the training budget increases. However, the relationship between FID and budget on the COCO validation set still follows a power-law

378  
379  
380  
381  
382  
383  
384  
385  
386  
387  
388  
389  
390  
391  
392  
393  
394  
395  
396  
397  
398  
399  
400  
401  
402  
403  
404  
405  
406  
407  
408  
409  
410  
411  
412  
413  
414  
415  
416  
417  
418  
419  
420  
421  
422  
423  
424  
425  
426  
427  
428  
429  
430  
431

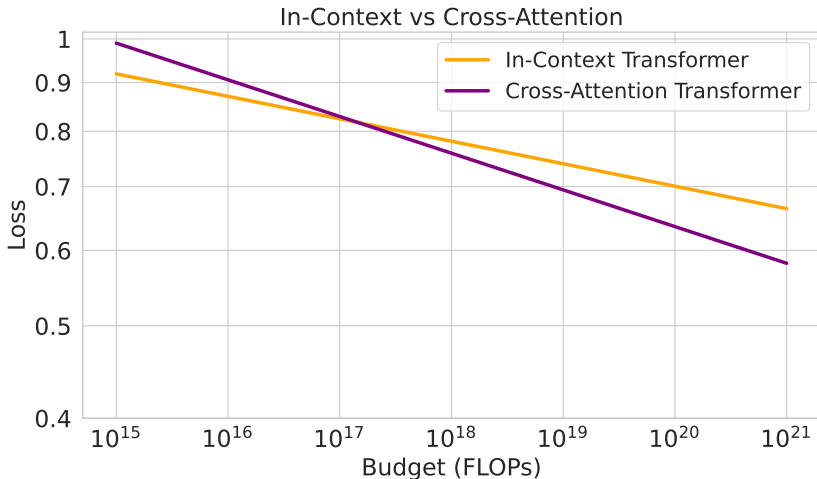


Figure 5: **Scaling curves for In-Context and Cross-Attention Transformers.** The plot compares the scaling behavior of In-Context Transformers and Cross-Attention Transformers with respect to compute budget (FLOPs). In-context transformers, which concatenate image, text, and time tokens, show a more gradual decline in loss compared to Cross-Attention Transformers, which inject time and text tokens via AdaLN and cross-attention blocks. The steeper slope of Cross-Attention Transformers indicates more efficient performance improvement with increasing compute, meaning they achieve lower loss with the same budget. These results highlight the efficiency of Cross-Attention Transformers and illustrate the potential of scaling laws in predicting performance trends across different model architectures.

trend. This suggests that, even on out-of-domain data, the FID-budget relationship can be reliably modeled using a power law, allowing us to predict the model’s FID for a given budget.

In summary, these results demonstrate that scaling laws are robust and can be applied effectively to out-of-domain datasets, maintaining consistent trends while accounting for dataset-specific performance differences. Despite the vertical offset in absolute performance, particularly in metrics like FID, the power-law relationships remain intact, allowing for reliable predictions of model performance under varying budgets. These findings highlight the potential of scaling laws as a versatile tool for understanding model behavior across datasets. The ability to project model efficiency and performance onto new data domains underscores the broader applicability of scaling laws in real-world scenarios.

#### 4 SCALING LAWS AS A PREDICTABLE BENCHMARK

Scaling laws offer a robust framework for evaluating the design quality of both models and datasets. Previous work such as Dubey et al. (2024); Bi et al. (2024) have all explored the scaling laws in data mix and quality. By modifying either the model architecture or the data pipeline, isoFLOP curves can be generated at smaller compute budgets to assess the impact of these changes. Specifically, after making adjustments to the model or dataset, experiments can be conducted across a range of smaller compute budgets, and the relationship between compute and metrics such as loss, parameter count, or token count can be fitted. The effectiveness of these modifications can then be evaluated by analyzing the exponents derived from the power-law fits.

Our evaluation follows three key principles:

- **Model improvements:** With a fixed dataset, a more efficient model will exhibit a lower model scaling exponent and a higher data scaling exponent. This suggests that the model can more effectively utilize the available data, allowing for a greater focus on increasing the dataset size with additional compute resources.



- **Data improvements:** When the model is fixed, a higher-quality dataset will result in a lower data scaling exponent and a higher model scaling exponent. This implies that a better dataset enables the model to scale more efficiently, yielding superior results with fewer resources.
- **Loss improvements:** Across both model and data modifications, an improved training pipeline is reflected in a smaller loss scaling exponent relative to compute. This indicates that the model achieves better performance with less compute, signaling overall gains in training efficiency.

The scaling trends for both models, In-Context Transformers and Cross-Attention Transformers, are clearly illustrated in Fig. 5. The loss scaling curves demonstrate that as the compute budget increases, the performance of both models improves, but at different rates. The Cross-Attention Transformer shows a steeper decline in loss compared to the In-Context Transformer, indicating that it achieves better performance with the same amount of compute.

The fitted scaling curves, as summarized in Tab. 1, support this observation. The Cross-Attention Transformer exhibits a larger model exponent, meaning that as compute budgets increase, more resources should be allocated toward scaling the dataset. Additionally, the smaller loss exponent of the Cross-Attention Transformer suggests a more rapid decline in loss, indicating that this model achieves superior performance compared to the In-Context Transformer. These findings align with the conclusions of Peebles & Xie (2023).

Model	Model Exponent	Data Exponent	Loss Exponent
In-context	0.56	0.43	-0.0273
Cross-Attention	0.54	0.46	-0.0385

Table 1: Exponents of model, data, and loss for different model architectures.

This example illustrates how scaling laws can serve as a reliable and predictable benchmark for evaluating the effectiveness of both model architectures and datasets. By analyzing the scaling exponents, we can draw meaningful conclusions about the potential and efficiency of different design choices in model and data pipelines.

## 5 DISCUSSION

**Limitations** While our work demonstrates the presence of scaling laws in Diffusion Transformers (DiT), several limitations must be acknowledged. First, we used fixed hyperparameters, such as learning rate and batch size, across all experiments. A more comprehensive investigation into how these parameters should be adjusted as budgets scale may lead to more precise predictions. Second, our study focuses solely on text-to-image generation, leaving the scalability of Diffusion Transformers with other data modalities, such as video, unexplored. Finally, we limited our analysis to In-Context Transformers and Cross-Attention Transformers, leaving the evaluation of additional model variants to future research.

**Conclusion** In this work, we explored the scaling laws of Diffusion Transformers (DiT) across a broad range of compute budgets, from  $1e17$  to  $6e18$  FLOPs, and confirmed the existence of a power-law relationship between pretraining loss and compute. This relationship enables precise predictions of optimal model size, data requirements, and model performance, even for large-scale budgets such as  $1e21$  FLOPs. Furthermore, we demonstrated the robustness of these scaling laws across different datasets, illustrating their generalizability beyond specific data distributions. In terms of generation performance, we showed that training budgets can be used to predict the visual quality of generated images, as measured by metrics like FID. Additionally, by testing both In-context Transformers and Cross-Attention Transformers, we validated the potential of scaling laws to serve as a predictable benchmark for evaluating and optimizing both model and data design, providing valuable guidance for future developments in text-to-image generation using DiT.

## REFERENCES

- 486  
487  
488 Josh Achiam, Steven Adler, Sandhini Agarwal, Lama Ahmad, Ilge Akkaya, Florencia Leoni Ale-  
489 man, Diogo Almeida, Janko Altenschmidt, Sam Altman, Shyamal Anadkat, et al. Gpt-4 technical  
490 report. *arXiv preprint arXiv:2303.08774*, 2023.
- 491 Michael S. Albergo, Nicholas M. Boffi, and Eric Vanden-Eijnden. Stochastic interpolants: A uni-  
492 fying framework for flows and diffusions, 2023. URL <https://arxiv.org/abs/2303.08797>.
- 493  
494 Fan Bao, Shen Nie, Kaiwen Xue, Yue Cao, Chongxuan Li, Hang Su, and Jun Zhu. All are worth  
495 words: A vit backbone for diffusion models. In *2023 IEEE/CVF Conference on Computer Vision*  
496 *and Pattern Recognition (CVPR)*. IEEE, June 2023. doi: 10.1109/cvpr52729.2023.02171. URL  
497 <http://dx.doi.org/10.1109/CVPR52729.2023.02171>.
- 498  
499 Xiao Bi, Deli Chen, Guanting Chen, Shanhuang Chen, Damai Dai, Chengqi Deng, Honghui Ding,  
500 Kai Dong, Qiushi Du, Zhe Fu, et al. Deepseek llm: Scaling open-source language models with  
501 longtermism. *arXiv preprint arXiv:2401.02954*, 2024.
- 502  
503 Junsong Chen, Jincheng Yu, Chongjian Ge, Lewei Yao, Enze Xie, Yue Wu, Zhongdao Wang, James  
504 Kwok, Ping Luo, Huchuan Lu, and Zhenguo Li. Pixart-: Fast training of diffusion transformer  
505 for photorealistic text-to-image synthesis, 2023.
- 506  
507 Ricky T. Q. Chen, Yulia Rubanova, Jesse Bettencourt, and David Duvenaud. Neural ordinary dif-  
508 ferential equations, 2019. URL <https://arxiv.org/abs/1806.07366>.
- 509  
510 Mostafa Dehghani, Josip Djolonga, Basil Mustafa, Piotr Padlewski, Jonathan Heek, Justin Gilmer,  
511 Andreas Peter Steiner, Mathilde Caron, Robert Geirhos, Ibrahim Alabdulmohsin, et al. Scaling  
512 vision transformers to 22 billion parameters. In *International Conference on Machine Learning*,  
pp. 7480–7512. PMLR, 2023.
- 513  
514 Jacob Devlin, Ming-Wei Chang, Kenton Lee, and Kristina Toutanova. Bert: Pre-training of deep  
515 bidirectional transformers for language understanding, 2019. URL <https://arxiv.org/abs/1810.04805>.
- 516  
517 Prafulla Dhariwal and Alex Nichol. Diffusion models beat gans on image synthesis, 2021. URL  
518 <https://arxiv.org/abs/2105.05233>.
- 519  
520 Laurent Dinh, Jascha Sohl-Dickstein, and Samy Bengio. Density estimation using real nvp, 2017.  
URL <https://arxiv.org/abs/1605.08803>.
- 521  
522 Alexey Dosovitskiy, Lucas Beyer, Alexander Kolesnikov, Dirk Weissenborn, Xiaohua Zhai, Thomas  
523 Unterthiner, Mostafa Dehghani, Matthias Minderer, Georg Heigold, Sylvain Gelly, Jakob Uszko-  
524 reit, and Neil Houlsby. An image is worth 16x16 words: Transformers for image recognition at  
525 scale, 2021. URL <https://arxiv.org/abs/2010.11929>.
- 526  
527 Abhimanyu Dubey, Abhinav Jauhri, Abhinav Pandey, Abhishek Kadian, Ahmad Al-Dahle, Aiesha  
528 Letman, Akhil Mathur, Alan Schelten, Amy Yang, Angela Fan, et al. The llama 3 herd of models.  
*arXiv preprint arXiv:2407.21783*, 2024.
- 529  
530 Patrick Esser, Sumith Kulal, Andreas Blattmann, Rahim Entezari, Jonas Müller, Harry Saini, Yam  
531 Levi, Dominik Lorenz, Axel Sauer, Frederic Boesel, Dustin Podell, Tim Dockhorn, Zion Eng-  
532 lish, Kyle Lacey, Alex Goodwin, Yannik Marek, and Robin Rombach. Scaling rectified flow  
533 transformers for high-resolution image synthesis, 2024.
- 534  
535 Shanghua Gao, Pan Zhou, Ming-Ming Cheng, and Shuicheng Yan. Masked diffusion transformer  
536 is a strong image synthesizer. In *2023 IEEE/CVF International Conference on Computer Vision*  
537 *(ICCV)*, pp. 23107–23116. IEEE, October 2023. doi: 10.1109/iccv51070.2023.02117. URL  
<http://dx.doi.org/10.1109/ICCV51070.2023.02117>.
- 538  
539 Will Grathwohl, Ricky T. Q. Chen, Jesse Bettencourt, Ilya Sutskever, and David Duvenaud. Ffjord:  
Free-form continuous dynamics for scalable reversible generative models, 2018. URL <https://arxiv.org/abs/1810.01367>.

- 540 Kaiming He, Xinlei Chen, Saining Xie, Yanghao Li, Piotr Dollár, and Ross Girshick. Masked  
541 autoencoders are scalable vision learners, 2021. URL <https://arxiv.org/abs/2111.06377>.  
542
- 543 Tom Henighan, Jared Kaplan, Mor Katz, Mark Chen, Christopher Hesse, Jacob Jackson, Hee-  
544 woo Jun, Tom B. Brown, Prafulla Dhariwal, Scott Gray, Chris Hallacy, Benjamin Mann, Alec  
545 Radford, Aditya Ramesh, Nick Ryder, Daniel M. Ziegler, John Schulman, Dario Amodei, and  
546 Sam McCandlish. Scaling laws for autoregressive generative modeling, 2020. URL <https://arxiv.org/abs/2010.14701>.  
547
- 548 Joel Hestness, Sharan Narang, Newsha Ardalani, Gregory Diamos, Heewoo Jun, Hassan Kianinejad,  
549 Md. Mostofa Ali Patwary, Yang Yang, and Yanqi Zhou. Deep learning scaling is predictable,  
550 empirically, 2017.  
551
- 552 Jonathan Ho and Tim Salimans. Classifier-free diffusion guidance, 2022. URL <https://arxiv.org/abs/2207.12598>.  
553
- 554 Jonathan Ho, Ajay Jain, and Pieter Abbeel. Denoising diffusion probabilistic models, 2020. URL  
555 <https://arxiv.org/abs/2006.11239>.  
556
- 557 Jordan Hoffmann, Sebastian Borgeaud, Arthur Mensch, Elena Buchatskaya, Trevor Cai, Eliza  
558 Rutherford, Diego de Las Casas, Lisa Anne Hendricks, Johannes Welbl, Aidan Clark, Tom Hen-  
559 nigan, Eric Noland, Katie Millican, George van den Driessche, Bogdan Damoc, Aurelia Guy,  
560 Simon Osindero, Karen Simonyan, Erich Elsen, Jack W. Rae, Oriol Vinyals, and Laurent Sifre.  
561 Training compute-optimal large language models, 2022.  
562
- 563 Jared Kaplan, Sam McCandlish, Tom Henighan, Tom B. Brown, Benjamin Chess, Rewon Child,  
564 Scott Gray, Alec Radford, Jeffrey Wu, and Dario Amodei. Scaling laws for neural language  
565 models, 2020. URL <https://arxiv.org/abs/2001.08361>.  
566
- 567 Diederik P. Kingma and Jimmy Ba. Adam: A method for stochastic optimization, 2017. URL  
568 <https://arxiv.org/abs/1412.6980>.  
569
- 570 Diederik P. Kingma and Prafulla Dhariwal. Glow: Generative flow with invertible 1x1 convolutions,  
571 2018. URL <https://arxiv.org/abs/1807.03039>.  
572
- 573 Diederik P Kingma and Max Welling. Auto-encoding variational bayes, 2022. URL <https://arxiv.org/abs/1312.6114>.  
574
- 575 Diederik P. Kingma, Tim Salimans, Ben Poole, and Jonathan Ho. Variational diffusion models,  
576 2021.  
577
- 578 Hao Li, Yang Zou, Ying Wang, Orchid Majumder, Yusheng Xie, R. Manmatha, Ashwin Swami-  
579 nathan, Zhuowen Tu, Stefano Ermon, and Stefano Soatto. On the scalability of diffusion-based  
580 text-to-image generation, 2024.  
581
- 582 Tsung-Yi Lin, Michael Maire, Serge Belongie, Lubomir Bourdev, Ross Girshick, James Hays, Pietro  
583 Perona, Deva Ramanan, C. Lawrence Zitnick, and Piotr Dollár. Microsoft coco: Common objects  
584 in context, 2015. URL <https://arxiv.org/abs/1405.0312>.  
585
- 586 Yaron Lipman, Ricky T. Q. Chen, Heli Ben-Hamu, Maximilian Nickel, and Matt Le. Flow matching  
587 for generative modeling, 2022.  
588
- 589 Haotian Liu, Chunyuan Li, Yuheng Li, and Yong Jae Lee. Improved baselines with visual instruction  
590 tuning, 2024. URL <https://arxiv.org/abs/2310.03744>.  
591
- 592 Xingchao Liu, Chengyue Gong, and Qiang Liu. Flow straight and fast: Learning to generate and  
593 transfer data with rectified flow, 2022.
- 590 Ilya Loshchilov and Frank Hutter. Decoupled weight decay regularization, 2019. URL <https://arxiv.org/abs/1711.05101>.  
591
- 592 Zeyu Lu, Zidong Wang, Di Huang, Chengyue Wu, Xihui Liu, Wanli Ouyang, and Lei Bai. Fit:  
593 Flexible vision transformer for diffusion model, 2024.

- 594 Nanye Ma, Mark Goldstein, Michael S. Albergo, Nicholas M. Boffi, Eric Vanden-Eijnden, and  
595 Saining Xie. Sit: Exploring flow and diffusion-based generative models with scalable interpolant  
596 transformers, 2024. URL <https://arxiv.org/abs/2401.08740>.
- 597 Kangfu Mei, Zhengzhong Tu, Mauricio Delbracio, Hossein Talebi, Vishal M. Patel, and Peyman  
598 Milanfar. Bigger is not always better: Scaling properties of latent diffusion models, 2024.
- 600 Igor Molybog, Peter Albert, Moya Chen, Zachary DeVito, David Esiobu, Naman Goyal, Punit Singh  
601 Koura, Sharan Narang, Andrew Poulton, Ruan Silva, Binh Tang, Diana Liskovich, Puxin Xu,  
602 Yuchen Zhang, Melanie Kambadur, Stephen Roller, and Susan Zhang. A theory on adam insta-  
603 bility in large-scale machine learning, 2023.
- 604 William Peebles and Saining Xie. Scalable diffusion models with transformers. In *2023*  
605 *IEEE/CVF International Conference on Computer Vision (ICCV)*. IEEE, October 2023. doi: 10.  
606 1109/iccv51070.2023.00387. URL [http://dx.doi.org/10.1109/ICCV51070.2023.](http://dx.doi.org/10.1109/ICCV51070.2023.00387)  
607 00387.
- 608 Ethan Perez, Florian Strub, Harm de Vries, Vincent Dumoulin, and Aaron Courville. Film: Visual  
609 reasoning with a general conditioning layer, 2017. URL [https://arxiv.org/abs/1709.](https://arxiv.org/abs/1709.07871)  
610 07871.
- 611 Alec Radford. Improving language understanding by generative pre-training. 2018.
- 612 Alec Radford, Jeff Wu, Rewon Child, David Luan, Dario Amodei, and Ilya Sutskever. Language  
613 models are unsupervised multitask learners. 2019.
- 614 Aditya Ramesh, Mikhail Pavlov, Gabriel Goh, Scott Gray, Chelsea Voss, Alec Radford, Mark Chen,  
615 and Ilya Sutskever. Zero-shot text-to-image generation, 2021.
- 616 Robin Rombach, Andreas Blattmann, Dominik Lorenz, Patrick Esser, and Björn Ommer. High-  
617 resolution image synthesis with latent diffusion models, 2022. URL [https://arxiv.org/](https://arxiv.org/abs/2112.10752)  
618 [abs/2112.10752](https://arxiv.org/abs/2112.10752).
- 619 Axel Sauer, Kashyap Chitta, Jens Müller, and Andreas Geiger. Projected gans converge faster, 2021.
- 620 Christoph Schuhmann, Romain Beaumont, Richard Vencu, Cade Gordon, Ross Wightman, Mehdi  
621 Cherti, Theo Coombes, Aarush Katta, Clayton Mullis, Mitchell Wortsman, Patrick Schramowski,  
622 Srivatsa Kundurthy, Katherine Crowson, Ludwig Schmidt, Robert Kaczmarczyk, and Jenia Jitsev.  
623 Laion-5b: An open large-scale dataset for training next generation image-text models, 2022. URL  
624 <https://arxiv.org/abs/2210.08402>.
- 625 Jascha Sohl-Dickstein, Eric A. Weiss, Niru Maheswaranathan, and Surya Ganguli. Deep unsuper-  
626 vised learning using nonequilibrium thermodynamics, 2015.
- 627 Yang Song and Stefano Ermon. Generative modeling by estimating gradients of the data distribution,  
628 2020. URL <https://arxiv.org/abs/1907.05600>.
- 629 Yang Song, Conor Durkan, Iain Murray, and Stefano Ermon. Maximum likelihood training of score-  
630 based diffusion models, 2021a. URL <https://arxiv.org/abs/2101.09258>.
- 631 Yang Song, Jascha Sohl-Dickstein, Diederik P. Kingma, Abhishek Kumar, Stefano Ermon, and Ben  
632 Poole. Score-based generative modeling through stochastic differential equations, 2021b. URL  
633 <https://arxiv.org/abs/2011.13456>.
- 634 Keqiang Sun, Junting Pan, Yuying Ge, Hao Li, Haodong Duan, Xiaoshi Wu, Renrui Zhang, Aojun  
635 Zhou, Zipeng Qin, Yi Wang, Jifeng Dai, Yu Qiao, Limin Wang, and Hongsheng Li. Journeydb:  
636 A benchmark for generative image understanding, 2023.
- 637 Chameleon Team. Chameleon: Mixed-modal early-fusion foundation models, 2024.
- 638 Arash Vahdat, Karsten Kreis, and Jan Kautz. Score-based generative modeling in latent space, 2021.
- 639 Ashish Vaswani, Noam Shazeer, Niki Parmar, Jakob Uszkoreit, Llion Jones, Aidan N. Gomez,  
640 Lukasz Kaiser, and Illia Polosukhin. Attention is all you need, 2023. URL [https://arxiv.](https://arxiv.org/abs/1706.03762)  
641 [org/abs/1706.03762](https://arxiv.org/abs/1706.03762).

648 Mitchell Wortsman, Peter J. Liu, Lechao Xiao, Katie Everett, Alex Alemi, Ben Adlam, John D. Co-  
649 Reyes, Izzeddin Gur, Abhishek Kumar, Roman Novak, Jeffrey Pennington, Jascha Sohl-dickstein,  
650 Kelvin Xu, Jaehoon Lee, Justin Gilmer, and Simon Kornblith. Small-scale proxies for large-scale  
651 transformer training instabilities, 2023.

652  
653 Biao Zhang and Rico Sennrich. Root mean square layer normalization, 2019.

654  
655 Hongkai Zheng, Weili Nie, Arash Vahdat, and Anima Anandkumar. Fast training of diffusion models  
656 with masked transformers, 2023.

657  
658  
659  
660  
661  
662  
663  
664  
665  
666  
667  
668  
669  
670  
671  
672  
673  
674  
675  
676  
677  
678  
679  
680  
681  
682  
683  
684  
685  
686  
687  
688  
689  
690  
691  
692  
693  
694  
695  
696  
697  
698  
699  
700  
701